nature

https://doi.org/10.1038/s41586-020-2180-5

Accelerated Article Preview

Structure of the SARS-CoV-2 spike receptor-binding domain bound to the ACE2 receptor

Received: 19 February 2020

Accepted: 19 March 2020

Accelerated Article Preview Published online 30 March 2020

Cite this article as: Lan, J. et al. Structure of the SARS-CoV-2 spike receptor-binding domain bound to the ACE2 receptor. *Nature* https://doi.org/10.1038/s41586-020-2180-5 (2020).

Jun Lan, Jiwan Ge, Jinfang Yu, Sisi Shan, Huan Zhou, Shilong Fan, Qi Zhang, Xuanling Shi, Qisheng Wang, Linqi Zhang & Xinquan Wang

Article

Structure of the SARS-CoV-2 spike receptor-binding domain bound to the ACE2 receptor

https://doi.org/10.1038/s41586-020-2180-5

Received: 19 February 2020

Accepted: 19 March 2020

Published online: 30 March 2020

Jun Lan[1,4], Jiwan Ge[1,4], Jinfang Yu[1,4], Sisi Shan[2,4], Huan Zhou[3], Shilong Fan[1], Qi Zhang[2], Xuanling Shi[2], Qisheng Wang[3], Linqi Zhang[2]✉ & Xinquan Wang[1]✉

A novel and highly pathogenic coronavirus (SARS-CoV-2) has caused an outbreak in Wuhan city, Hubei province of China since December 2019, and soon spread nationwide and spilled over to other countries around the world[1–3]. To better understand the initial step of infection at an atomic level, we determined the crystal structure of the SARS-CoV-2 spike receptor-binding domain (RBD) bound to the cell receptor ACE2 at 2.45 Å resolution. The overall ACE2-binding mode of the SARS-CoV-2 RBD is nearly identical to that of the SARS-CoV RBD, which also utilizes ACE2 as the cell receptor[4]. Structural analysis identified residues in the SARS-CoV-2 RBD that are critical for ACE2 binding, the majority of which either are highly conserved or share similar side chain properties with those in the SARS-CoV RBD. Such similarity in structure and sequence strongly argue for convergent evolution between the SARS-CoV-2 and SARS-CoV RBDs for improved binding to ACE2, although SARS-CoV-2 does not cluster within SARS and SARS-related coronaviruses[1–3,5]. The epitopes of two SARS-CoV antibodies targeting the RBD are also analysed with the SARS-CoV-2 RBD, providing insights into the future identification of cross-reactive antibodies.

The emergence of a novel and highly pathogenic coronavirus (SARS-CoV-2) in Wuhan city, Hubei province of China and its rapid international spread has posed a serious global public health emergency[1–3]. Similar to those infected by pathogenic severe acute respiratory syndrome coronavirus (SARS-CoV) in 2003 and Middle East respiratory syndrome coronavirus (MERS-CoV) in 2012, patients infected by SARS-CoV-2 manifested a range of symptoms including dry cough, fever, headache, dyspnea and pneumonia with estimated mortality rate in the range of 3–5%[6–8]. Since the initial outbreak in December of 2019, SARS-CoV-2 has spread throughout China and to more than eighty other countries and areas worldwide. As of March 5, 2020, 80,565 cases in China have been confirmed with the infection and 3,015 infected patients have died (https://www.who.int/emergencies/diseases/novel-coronavirus-2019/situation-reports/). Currently, the epicentre Wuhan and the neighbouring cities have been under lockdown to minimize continued spread, and the WHO has announced a Public Health Emergency of International Concern (PHEIC) duo to the rapid and global dissemination of SARS-CoV-2.

Phylogenetic analysis on the coronavirus genomes has revealed that SARS-CoV-2 is a new member of the betacoronavirus genus, which includes SARS-CoV, MERS-CoV, bat SARS-related coronaviruses (SARSr-CoV), as well as others identified in humans and diverse animal species[1–3,5]. Bat coronavirus RaTG13 appears to be the closest relative of the SARS-CoV-2 sharing over 93.1% sequence identity in the spike (S) gene. SARS-CoV and other SARSr-CoVs however are rather distinct with less than 80% sequence identity[1].

Coronaviruses utilize the homotrimeric spike glycoprotein (S1 subunit and S2 subunit in each spike monomer) on the envelope to bind their cellular receptors. Such binding triggers a cascade of events leading to the fusion between cell and viral membranes for cell entry. Previous cryo-EM studies of the SARS-CoV spike and its interaction with the cell receptor ACE2 have shown that the receptor binding induces the dissociation of the S1 with ACE2, prompting the S2 to transit from a metastable prefusion to a more stable postfusion state essential for membrane fusion[9–12]. Therefore, binding to ACE2 receptor is a critical initial step for the SARS-CoV to enter into target cells. Recent studies also pointed to the important role of ACE2 in mediating entry of SARS-CoV-2[1,13–15]. HeLa cells expressing ACE2 are susceptible to SARS-CoV-2 infection while those without failed to do so[1]. In vitro binding measurements also showed that the SARS-CoV-2 RBD binds to ACE2 with an affinity in the low nM range, indicating that the RBD is the key functional component within the S1 subunit responsible for binding of SARS-CoV-2 by ACE2[13,16].

The cryo-EM structure of the SARS-CoV-2 spike trimer has just been reported in two independent studies[13,17]. However, inspection of one available spike structure revealed incomplete modelling of the RBD, particularly for the receptor-binding motif (RBM) that interacts directly with ACE2[17]. Computer modelling of interaction between SARS-CoV-2 RBD and ACE2 has identified some residues potentially involved in the interaction but the actual interaction remained elusive[18]. Furthermore, despite of detectable cross-reactive neutralizing activity from serum/plasma of SARS-CoV recovered patients[15], no SARS-CoV monoclonal antibodies targeted to RBD so far isolated are able to bind and neutralize

[1]The Ministry of Education Key Laboratory of Protein Science, Beijing Advanced Innovation Center for Structural Biology, Beijing Frontier Research Center for Biological Structure, Collaborative Innovation Center for Biotherapy, School of Life Sciences, Tsinghua University, 100084, Beijing, China. [2]Center for Global Health and Infectious Diseases, Comprehensive AIDS Research Center, and Beijing Advanced Innovation Center for Structural Biology, School of Medicine, Tsinghua University, Beijing, 100084, China. [3]Shanghai Synchrotron Radiation Facility, Shanghai Advanced Research Institute, Chinese Academy of Sciences, Shanghai, 201204, China. [4]These authors contributed equally: Jun Lan, Jiwan Ge, Jinfang Yu, Sisi Shan. ✉e-mail: zhanglinqi@mail.tsinghua.edu.cn; xinquanwang@mail.tsinghua.edu.cn

SARS-CoV-2[16,17]. These findings highlight some intrinsic sequence and structure differences between the SARS-CoV and SARS-CoV-2 RBDs.

To elucidate the SARS-CoV-2 RBD and ACE2 interaction at a higher resolution, we chose to determine the complex structure of SARS-CoV-2 RBD bound with ACE2 by X-ray crystallography. The atomic-level structural information would greatly improve our understanding of interaction between SARS-CoV-2 and susceptible cells, providing precise target for neutralizing antibodies, and assisting structure-based vaccine design urgently needed in our ongoing combat against SARS-CoV-2. Specifically, we expressed the SARS-CoV-2 RBD (residues Arg319-Phe541) (Fig. 1a, b) and the N-terminal peptidase domain of ACE2 (residues Ser19-Asp615) in Hi5 insect cells and purified them by Ni-NTA affinity and gel-filtration (Extended Data Fig. 1). The complex structure was determined by molecular replacement using the SARS-CoV RBD and ACE2 structures as search models[4], and refined at 2.45 Å resolution to final R_{work} and R_{free} factors of 19.6% and 23.7%, respectively (Extended Data Fig. 2 and Extended Data Table 1). The final model contains residues Thr333 to Gly526 of the SARS-CoV-2 RBD, residues Ser19 to Asp615 of the ACE2 N-terminal peptidase domain, one zinc ion, four NAG glycans linked to ACE2 Asn90, Asn322 and Asn546 and to RBD Asn343, as well as 80 water molecules.

The SARS-CoV-2 RBD has a twisted five-stranded antiparallel β sheet (β1, β2, β3, β4 and β7) with short connecting helices and loops forming as the core (Fig. 1b, c). Between the β4 and β7 strands in the core, there is an extended insertion containing short β5 and β6 strands, α4 and α5 helices and loops (Fig. 1b, c). This extended insertion is the receptor-binding motif (RBM) containing most of the contacting residues of SARS-CoV-2 for ACE2 binding. A total of nine cysteine residues are found in the RBD, eight of which forming four pairs of disulfide bonds are resolved in the final model. Among these four pairs, three are in the core (Cys336-Cys361, Cys379-Cys432 and Cys391-Cys525) to help stabilize the β sheet structure (Fig. 1c) while the remaining one (Cys480-Cys488) connects loops in the distal end of the RBM (Fig. 1c). The N-terminal peptidase domain of ACE2 has two lobes, forming the peptide substrate binding site between them. The extended RBM in the SARS-CoV-2 RBD contacts the bottom side of the ACE2 small lobe, with a concave outer surface in the RBM accommodating the N-terminal helix of the ACE2 (Fig. 1c). The overall structure of the SARS-CoV-2 RBD is similar to that of the SARS-CoV RBD (Extended Data Fig. 3a), with an r.m.s.d. of 1.2 Å for 174 aligned Cα atoms. Even in the RBM that has more sequence variations, the overall structure is also highly similar (r.m.s.d. of 1.3 Å) with only one obvious conformational change in the distal end (Extended Data Fig. 3a). The overall binding mode of the SARS-CoV-2 RBD to the ACE2 is also nearly identical to that observed in previously determined SARS-CoV RBD-ACE2 complex structure[4] (Extended Data Fig. 3b).

The cradling of the ACE2 N-terminal helix by the RBM outer surface results in a large buried surface of 1687 Å^2 (864 Å^2 on the RBD and 823 Å^2 on the ACE2) at the SARS-CoV-2 RBD/ACE2 interface. Nearly the same buried surface of 1699 Å^2 contributed by SARS-CoV RBD (869 Å^2) and ACE2 (830 Å^2) is also observed at the SARS-CoV RBD/ACE2 interface. With a distance cutoff of 4 Å, a total of 17 residues of the RBD contact 20 residues of the ACE2 (Fig. 2a and Extended Data Table 2). Analysis of interface between SARS-CoV RBD and ACE2 revealed a total of 16 residues of the SARS-CoV RBD contact 20 residues of the ACE2 (Fig. 2a and Extended Data Table 2). Among the 20 ACE2 residues interacting with the two different RBDs, 17 residues are shared and most of which are located at the N-terminal helix (Fig. 2a and Extended Data Table 2).

To compare the ACE2-interacting residues on the SARS-CoV-2 and SARS-CoV RBDs, we used structure-guided sequence alignment and mapped them onto their respective sequences (Fig. 2b). Among 14 shared amino acid positions used by both RBMs for ACE2 interaction, eight have the identical residues between the SARS-CoV-2 and SARS-CoV RBDs including Tyr449/Tyr436, Tyr453/Tyr440, Asn487/Asn473, Tyr489/Tyr475, Gly496/Gly482, Thr500/Thr486, Gly502/Gly488 and Tyr505/Tyr491 (Fig. 2b). Five positions have residues demonstrating similar biochemical properties despite of having different side chains, including Leu455/Tyr442, Phe456/Leu443, 486Phe/Leu472, Gln493/Asn479 and Asn501/Thr487 (Fig. 2b). The remaining one is at the Gln498/Tyr484 position (Fig. 2b), at which the SARS-CoV-2 Gln498 and SARS-CoV Tyr484 both interacts with ACE2 Asp38, Tyr41, Gln42, Leu45 and Lys353. Among the six RBD positions with changed residues, SARS-CoV residues Tyr442, Leu472, Asn479 and Thr487 have previously been shown to be critical for binding ACE2[18]. At the Leu455/Tyr442 position, SARS-CoV-2 Leu455 and SARS-CoV Tyr442 have similar interactions with ACE2 Asp30, Lys31 and His34 (Fig. 3a). At the Phe486/Leu472 position, SARS-CoV-2 Phe486 interacts with ACE2 Gln24, Leu79, Met82 and Tyr83, and Leu472 has less interactions with ACE2 Leu79 and Met82 (Fig. 3a). At the Gln493/Asn479 position, SARS-CoV-2 Gln493 interacts with ACE2 Lys31, His34 and Glu35 and forms a hydrogen bond with Glu35, and SARS-CoV Asn479 only interacts with ACE2 His34 (Fig. 3a). At the Asn501/Thr487 position, both residues have similar interactions with ACE2 Tyr41, Lys353, Gly354 and Asp355 (Fig. 3a). SARS-CoV-2 Asn501 and SARS-CoV Thr487 both form a hydrogen-bond with ACE2 Tyr41 (Fig. 3a). Outside RBM, there is a unique ACE2-interacting residue Lys417 in the SARS-CoV-2, forming salt-bridge interactions with ACE2 Asp30 (Fig. 3b). This position is replaced by a valine in the SARS-CoV RBD that fails to participate in ACE2 binding (Figs. 2b, 3b). Consistently, comparison of the surface electrostatic potential also identified a positive-charged patch on the SARS-CoV-2 RBD contributed by Lys417 that is absent on the SARS-CoV RBD (Fig. 3b). These subtle different ACE2 interactions may contribute to the binding affinity difference of the SARS-CoV-2 and SARS-CoV to ACE2 receptor (4.7 nM vs 31 nM) (Extended Data Fig. 4).

One prominent and common feature presented at both RBD/ACE2 interfaces is the networks of hydrophilic interactions. There are 13 hydrogen bonds and 2 salt bridges at the SARS-CoV-2 RBD/ACE2 interface, and 13 hydrogen bonds and 3 salt bridges at the SARS-CoV RBD/ACE2 interface (Table 1). The second shared feature is the involvement of multiple tyrosine residues in forming hydrogen-bonding interactions with the polar hydroxyl group. These include Tyr449, Tyr489 and Tyr505 from the SARS-CoV-2 RBD and Tyr436, Tyr475 and Tyr491 from the SARS-CoV RBD (Table 1). The third shared feature may reside in the Asn90-linked glycans of the ACE2 in binding different RBDs. In the SARS-CoV RBD-ACE2 complex structure, a chain of Asn90-linked NAG-NAG-BMA contacts with Thr402 of the SARS-CoV RBD (Extended Data Fig. 5a), and this glycan-RBD interaction was proposed to play important roles in the binding of SARS-CoV RBD by ACE2[4,19]. In the SARS-CoV-2 RBD-ACE2 structure, the density only allowed the modelling of the first NAG linked to ACE2 Asn90, and no interactions between this NAG and the SARS-CoV-2 RBD were observed (Extended Data Fig. 5b). However, this does not exclude that glycans after the first NAG may interact with the SARS-CoV-2 RBD and may play important roles in the binding of SARS-CoV-2 RBD by ACE2. Taken together, the above described results show that the SARS-CoV-2 RBD/ACE2 and SARS-CoV RBD/ACE2 interfaces share substantial similarity in the buried surface area, the number of interacting residues, and hydrophilic interaction networks, although some different ACE2 interactions were observed both in and outside the RBM (Fig. 3a, b). Such similarity argues strongly for the convergent evolution of the SARS-CoV-2 and SARS-CoV RBD structures to improve binding affinity to the same ACE2 receptor, although SARS-CoV-2 does not cluster within SARS-CoV and SARSr-CoV in the betacoronavirus genus.

Consistent with high structural similarity, we found that the binding affinities between ACE2 and SARS-CoV-2 and SARS-CoV RBDs also fall into a similar range. Specifically, the K_D value between ACE2 and SARS-CoV-2 RBD is 4.7 nM, and that between ACE2 and SARS-CoV RBD is 31 nM (Extended Data Fig. 4). Similar results have also been reported by other groups[13,16]. However, this is somewhat different from a recent report

where a ~20 fold increased binding between ACE2 and SARS-CoV-2 spike trimer was found (K_D of 14.7 nM) compared with that between ACE2 and SARS-CoV RBD-SD1 (K_D of 325 nM)[17]. This is perhaps due to the different proteins used in the assay or some other unknown reasons. Nevertheless, the binding affinity alone is unlikely to explain the unusual transmissibility of SARS-CoV-2. Other factors such as the unique "RRAR" furin cleavage site at the S1/S2 boundary of the SARS-CoV-2 spike may play more important roles in facilitating the rapid human-to-human transmission.

Neutralizing antibodies represent a critical component of immune system in fighting against viral infection. It has been reported that the SARS-CoV-2 could be cross-neutralized by horse anti-SARS-CoV serum and convalescent serum from SARS-infected patient[1,15], reinforcing structural similarity between SARS-CoV-2 and SARS-CoV RBDs. Such similarity also raised the hope of rapid application of previously characterized SARS-CoV monoclonal antibodies in the clinical setting. However, no antibody targeted to SARS-CoV (m396, S230, 80R and CR3014) has so far demonstrated any impressive cross-binding and neutralization activity against SARS-CoV-2 spike or RBD[16,17,20–23]. One exception is SARS-CoV antibody CR3022 that binds to the SARS-CoV-2 RBD with a K_D of 6.2 nM, although its neutralizing activity against SARS-CoV-2 has not been reported yet[16]. Currently, we are uncertain where exactly the epitope of CR3022 on SARS-CoV nor on SARS-CoV-2 RBDs is. Among the three antibodies incapable of binding to the SARS-CoV-2 RBD, two (m396 and 80R) have the epitopes resolved by high resolution crystal structure determination of SARS-CoV RBD-Fab complexes[20,21]. Through mapping these epitope residues onto the sequence of SARS-CoV RBD aligned with the sequence of SARS-CoV-2 RBD (Fig. 4), we found that antibody m396 has seven residue changes in the SARS-CoV-2 RBD among 21 epitope positions (Fig. 4). There are 16 residue changes in the SARS-CoV-2 RBD among 25 epitope positions by antibody 80R (Fig. 4). This may provide the structural basis for the lack of cross-reactivity by m396 and 80R. The cross-neutralization of SARS-CoV-2 by horse anti-SARS-CoV serum and serum/plasm from recovered SARS patients indicates a great potential in identifying antibodies with cross-reactivity between these two coronaviruses[1,15]. The conserved non-RBD regions in the spike such as the S2 subunit are the potential targets for cross-reactive antibodies. Although the RBD is less conserved, identical residues between SARS-CoV-2 and SARS-CoV RBD indeed exist, even in the more variable RBM (Fig. 4). Considering that the RBD is the critical region for receptor binding, antibodies targeting the conserved epitopes in the RBD will also present a great promise for developing highly potent cross-reactive therapeutic agents towards diverse coronavirus species including SARS-CoV-2.

Online content

Any methods, additional references, Nature Research reporting summaries, source data, extended data, supplementary information, acknowledgements, peer review information; details of author contributions and competing interests; and statements of data and code availability are available at https://doi.org/10.1038/s41586-020-2180-5.

1. Zhou, P. et al. A pneumonia outbreak associated with a new coronavirus of probable bat origin. *Nature* **579**, 270–273 (2020). https://doi.org/10.1038/s41586-020-2012-7.
2. Wu, F. et al. A new coronavirus associated with human respiratory disease in China. *Nature* **579**, 265–269 (2020). https://doi.org/10.1038/s41586-020-2008-3.
3. Zhu, N. et al. A Novel Coronavirus from Patients with Pneumonia in China, 2019. *N. Engl. J. Med.* **382**, 727–733 (2020). https://doi.org/10.1056/NEJMoa2001017.
4. Li, F., Li, W., Farzan, M. & Harrison, S. C. Structure of SARS coronavirus spike receptor-binding domain complexed with receptor. *Science* **309**, 1864–1868 (2005). https://doi.org/10.1126/science.1116480.
5. Lu, R. et al. Genomic characterisation and epidemiology of 2019 novel coronavirus: implications for virus origins and receptor binding. *Lancet* **395**, 565–574 (2020). https://doi.org/10.1016/S0140-6736(20)30251-8.
6. Huang, C. et al. Clinical features of patients infected with 2019 novel coronavirus in Wuhan, China. *Lancet* **395**, 497–506 (2020). https://doi.org/10.1016/S0140-6736(20)30183-5.
7. Liu, K. et al. Clinical characteristics of novel coronavirus cases in tertiary hospitals in Hubei Province. *Chin. Med. J. (Engl.)* (2020). https://doi.org/10.1097/CM9.0000000000000744
8. Wang, D. et al. Clinical Characteristics of 138 Hospitalized Patients With 2019 Novel Coronavirus-Infected Pneumonia in Wuhan, China. *J. Am. Med. Assoc.* (2020). https://doi.org/10.1001/jama.2020.1585
9. Gui, M. et al. Cryo-electron microscopy structures of the SARS-CoV spike glycoprotein reveal a prerequisite conformational state for receptor binding. *Cell Res.* **27**, 119–129 (2017). https://doi.org/10.1038/cr.2016.152.
10. Song, W., Gui, M., Wang, X. & Xiang, Y. Cryo-EM structure of the SARS coronavirus spike glycoprotein in complex with its host cell receptor ACE2. *PLoS Pathog.* **14**, e1007236 (2018). https://doi.org/10.1371/journal.ppat.1007236.
11. Kirchdoerfer, R. N. et al. Stabilized coronavirus spikes are resistant to conformational changes induced by receptor recognition or proteolysis. *Sci. Rep.* **8**, 15701 (2018). https://doi.org/10.1038/s41598-018-34171-7.
12. Yuan, Y. et al. Cryo-EM structures of MERS-CoV and SARS-CoV spike glycoproteins reveal the dynamic receptor binding domains. *Nat. Commun.* **8**, 15092 (2017). https://doi.org/10.1038/ncomms15092.
13. Walls, A. C. et al. Structure, Function, and Antigenicity of the SARS-CoV-2 Spike Glycoprotein. *Cell* S0092-8674(20)30262-2 (2020). https://doi.org/10.1016/j.cell.2020.02.058
14. Letko, M., Marzi, A. & Munster, V. Functional assessment of cell entry and receptor usage for SARS-CoV-2 and other lineage B betacoronaviruses. *Nat. Microbiol.* (2020). https://doi.org/10.1038/s41564-020-0688-y
15. Hoffmann, M. et al. SARS-CoV-2 Cell Entry Depends on ACE2 and TMPRSS2 and Is Blocked by a Clinically Proven Protease Inhibitor. *Cell* S0092-8674(20)30229-4 (2020). https://doi.org/10.1016/j.cell.2020.02.052
16. Tian, X. et al. Potent binding of 2019 novel coronavirus spike protein by a SARS coronavirus-specific human monoclonal antibody. *Emerg. Microbes Infect.* **9**, 382–385 (2020). https://doi.org/10.1080/22221751.2020.1729069.
17. Wrapp, D. et al. Cryo-EM structure of the 2019-nCoV spike in the prefusion conformation. *Science* **367**, 1260–1263 (2020). https://doi.org/10.1126/science.abb2507.
18. Wan, Y., Shang, J., Graham, R., Baric, R. S. & Li, F. Receptor recognition by novel coronavirus from Wuhan: An analysis based on decade-long structural studies of SARS. *J. Virol.* **94**, e00127-20 (2020). https://doi.org/10.1128/JVI.00127-20.
19. Li, W. et al. Receptor and viral determinants of SARS-coronavirus adaptation to human ACE2. *EMBO J.* **24**, 1634–1643 (2005). https://doi.org/10.1038/sj.emboj.7600640.
20. Prabakaran, P. et al. Structure of severe acute respiratory syndrome coronavirus receptor-binding domain complexed with neutralizing antibody. *J. Biol. Chem.* **281**, 15829–15836 (2006). https://doi.org/10.1074/jbc.M600697200.
21. Hwang, W. C. et al. Structural basis of neutralization by a human anti-severe acute respiratory syndrome spike protein antibody, 80R. *J. Biol. Chem.* **281**, 34610–34616 (2006). https://doi.org/10.1074/jbc.M603275200.
22. Walls, A. C. *et al.* Unexpected Receptor Functional Mimicry Elucidates Activation of Coronavirus Fusion. *Cell* **176**, 1026–1039 e1015, https://doi.org/10.1016/j.cell.2018.12.028 (2019).
23. van den Brink, E. N. et al. Molecular and biological characterization of human monoclonal antibodies binding to the spike and nucleocapsid proteins of severe acute respiratory syndrome coronavirus. *J. Virol.* **79**, 1635–1644 (2005). https://doi.org/10.1128/JVI.79.3.1635-1644.2005.

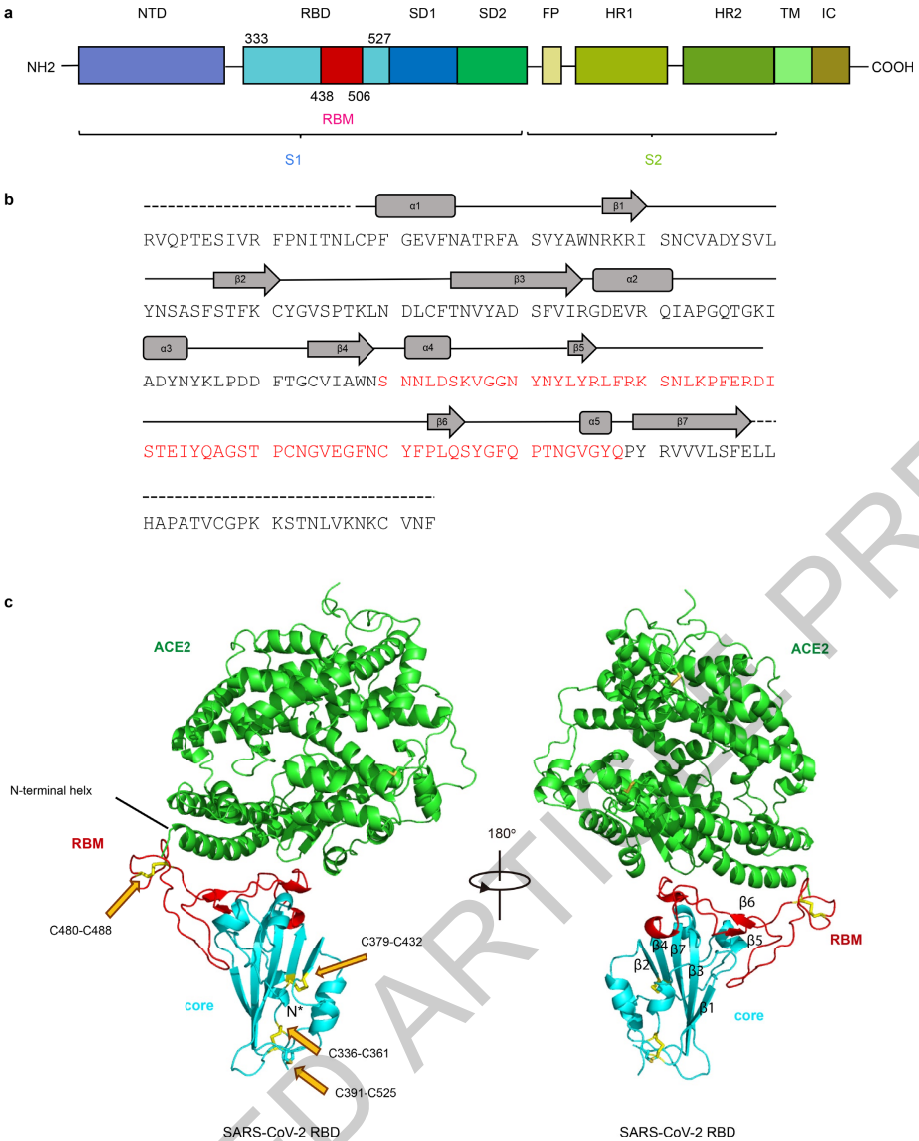

Fig. 1 | Overall structure of SARS-CoV-2 RBD bound with ACE2. a, Overall topology of SARS-CoV-2 spike monomer. NTD, N-terminal domain. RBD, receptor-binding domain. RBM, receptor-binding motif. SD1, subdomain 1. SD2, subdomain 2. FP, fusion peptide. HR1, heptad repeat 1. HR2, heptad repeat 2. TM, transmembrane region. IC, intracellular domain. **b**, Sequence and secondary structures of SARS-CoV-2 RBD. The RBM is colored red. **c**, Overall structure of SARS-CoV-2 RBD bound with ACE2. ACE2 is colored green. SARS-CoV-2 RBD core is colored cyan and RBM is colored red. Disulfide bonds in the SARS-CoV-2 RBD are shown as stick and indicated by yellow arrows. The N-terminal helix of ACE2 responsible for binding is labelled.

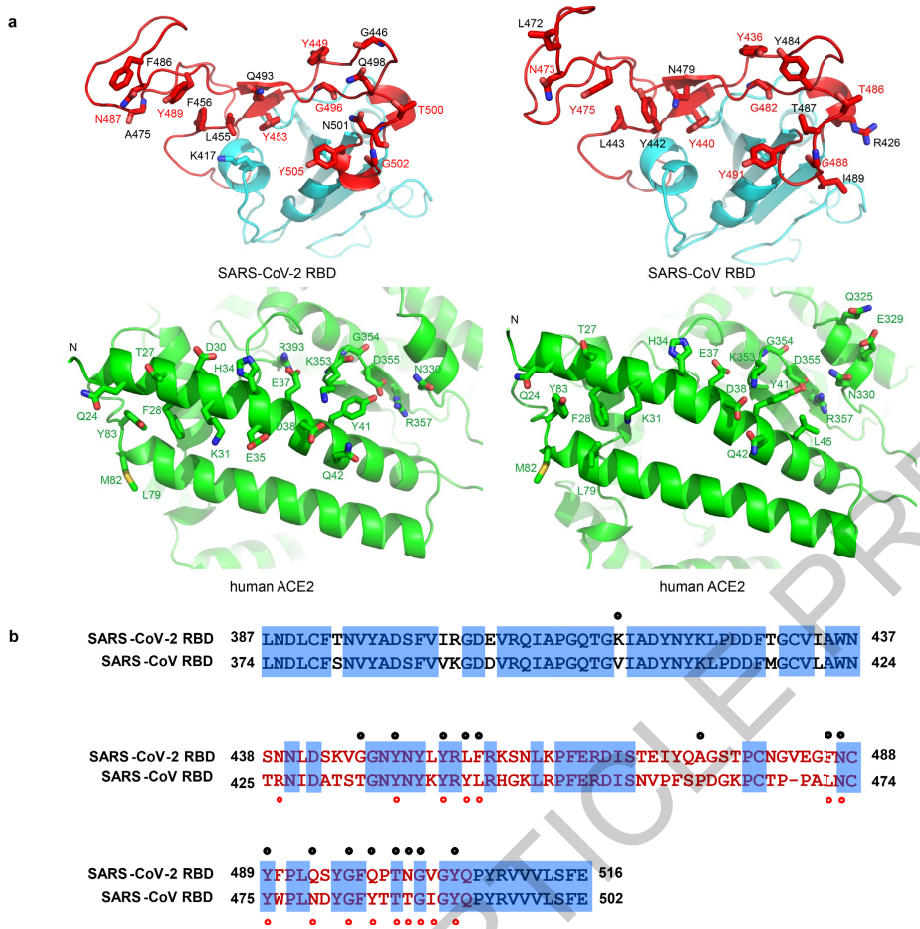

Fig. 2 | The SARS-CoV-2 RBD/ACE2 and SARS-CoV RBD/ACE2 interfaces. **a**, Contacting residues shown as stick at the SARS-CoV-2 RBD/ACE2 and SARS-CoV RBD/ACE2 interfaces. Positions in both RBDs involved in ACE2 binding are indicated by red labels. **b**, Sequence alignment of SARS-CoV-2 RBD and SARS-CoV RBD. Contacting residues in the SARS-CoV-2 RBD are indicated by black dots; contacting residues in the SARS-CoV RBD are indicated by red dots.

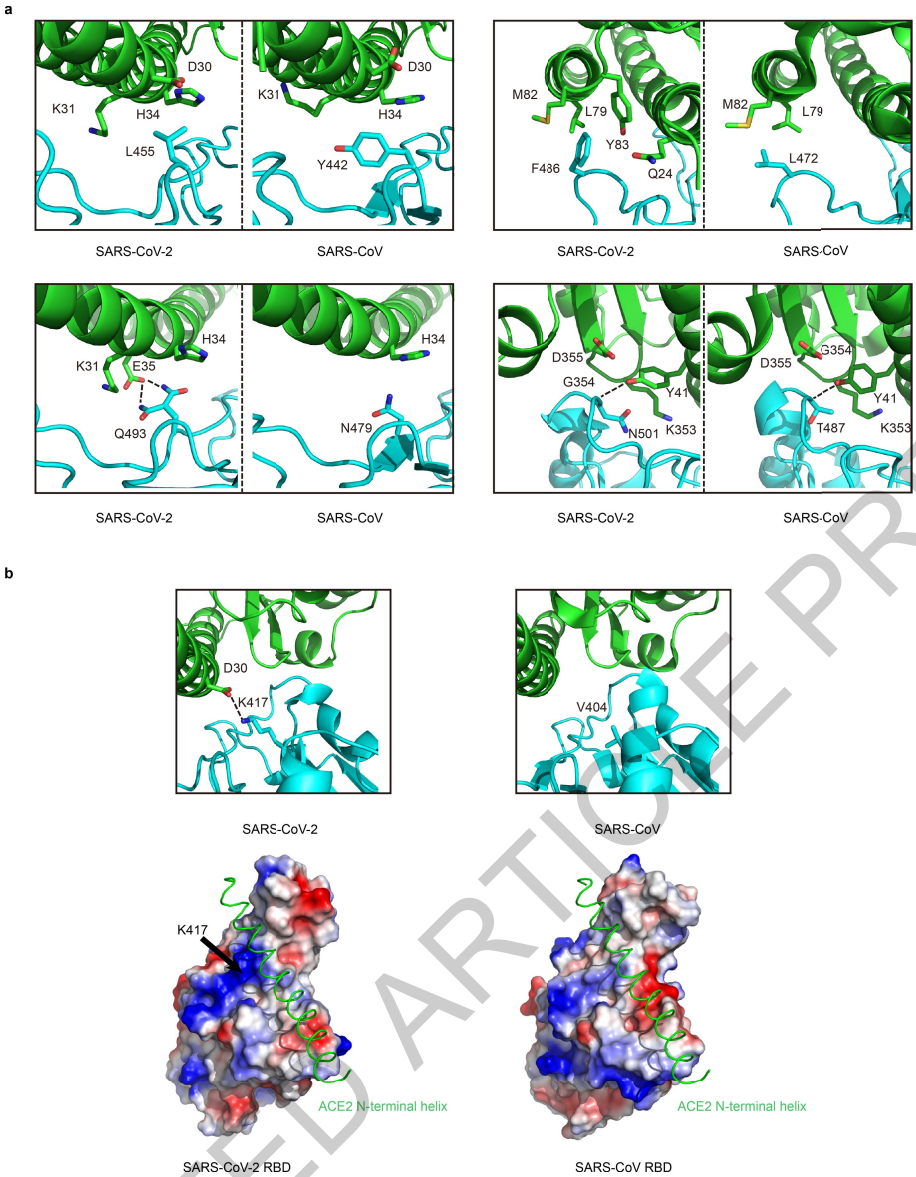

Fig. 3 | Comparisons of interactions at the SARS-CoV-2 RBD/ACE2 and SARS-CoV RBD/ACE2 interfaces. a, Interactions around the SARS-CoV-2 and SARS-CoV positions in the RBM with changed residues. SARS-CoV-2 and SARS-CoV RBDs are colored cyan. ACE2 is colored green. **b**, Interactions around the K417/V404 position outside the RBM and electrostatic potential maps of the SARS-CoV-2 and SARS-CoV RBDs. The position of K417 in the SARS-CoV-2 RBD is indicated by black arrow. The N-terminal helix of ACE2 is shown as green ribbon. The PDB code for SARS-CoV RBD-ACE2 complex: 2AJF.

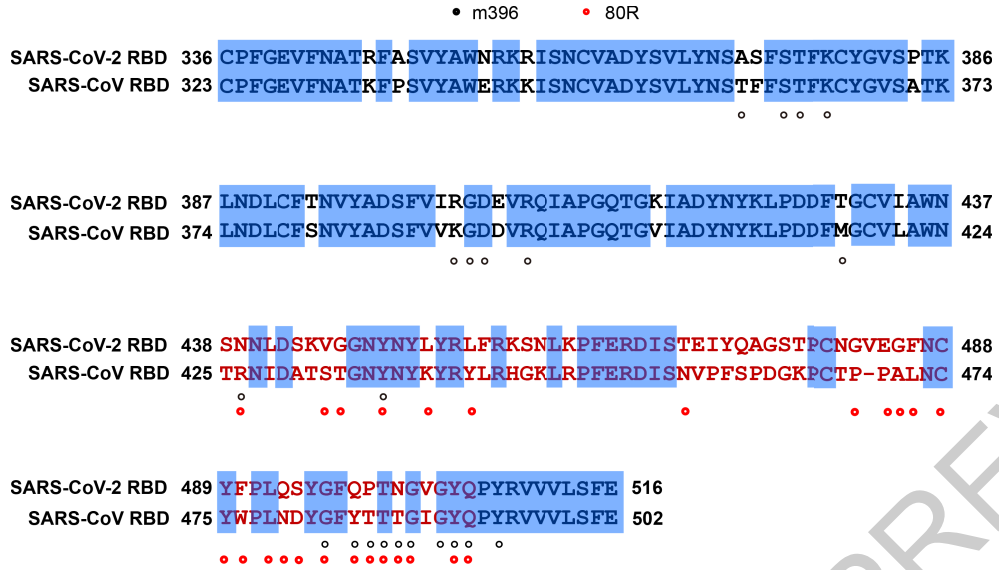

Fig. 4 | Mapping of SARS-CoV neutralizing antibody epitopes. The epitopes of SARS-CoV neutralizing antibodies m396 and 80R, which target the RBD, are labelled in the SARS-CoV sequence aligned with the sequence of SARS-CoV-2 RBD. Epitope residues of m396 are indicated by black dots; epitope residues of 80R are indicated by red dots.

Table 1 | The hydrogen bonds and salt bridges at the SARS-CoV-2 RBD/ACE2 and SARS-CoV RBD/ACE2 interfaces

	SARS-CoV-2 RBD	Length(Å)	ACE2	Length(Å)	SARS-CoV RBD
Hydrogen bonds	N487(ND2)	2.6	Q24(OE1)	2.9	N473(ND2)
	K417(NZ)	3.0	D30(OD2)		
	Q493(NE2)	2.8	E35(OE2)		
			E37(OE1)	3.4	Y491(OH)
	Y505(OH)	3.2	E37(OE2)		
			D38(OD1)	3.0	Y436(OH)
	Y449(OH)	2.7	D38(OD2)	3.0	Y436(OH)
	T500(OG1)	2.6	Y41(OH)	2.8	T486(OG1)
	N501(N)	3.7	Y41(OH)	3.3	T487(N)
	G446(O)	3.3	Q42(NE2)		
	Y449(OH)	3.0	Q42(NE2)		
			Q42(OE1)	2.7	Y436(OH)
	Y489(OH)	3.5	Y83(OH)	3.3	Y475(OH)
	N487(OD1)	2.7	Y83(OH)	2.8	N473(ND2)
			Q325(OE1)	3.8	R426(NH2)
			E329(OE2)	3.0	R426(NH2)
			N330(ND2)	2.8	T486(O)
	G502(N)	2.8	K353(O)	2.6	G488(N)
	Y505(OH)	3.7	R393(NH2)		
Salt bridges	K417(NZ)	3.9	D30(OD1)		
	K417(NZ)	3.0	D30(OD2)		
			E329(OE2)	3.7	R426(NH1)
			E329(OE1)	3.9	R426(NH2)
			E329(OE2)	3.0	R426(NH2)

Methods

Protein expression and purification

The SARS-CoV-2 receptor-binding domain (RBD) and the N-terminal peptidase domain of human ACE2 were expressed using the Bac-to-Bac baculovirus system (Invitrogen). The SARS-CoV-2 RBD (residues Arg319-Phe541) with an N-terminal gp67 signal peptide for secretion and a C-terminal 6 × His tag for purification was inserted into pFastBac-Dual vector (Invitrogen). The construct was transformed into bacterial DH10Bac competent cells, and the extracted bacmid was then transfected into Sf9 cells using Cellfectin II Reagent (Invitrogen). The low-titer viruses were harvested and then amplified to generate high-titer virus stock, which was used to infect Hi5 cells at a density of 2×10^6 cells/ml. The supernatant of cell culture containing the secreted RBD was harvested 60 h after infection, concentrated and buffer-exchanged to HBS (10 mM HEPES, pH 7.2, 150 mM NaCl). RBD was captured by Ni-NTA resin (GE Healthcare) and eluted with 500 mM imidazole in HBS buffer. RBD was then purified by gel filtration chromatography using the Superdex 200 column (GE Healthcare) pre-equilibrated with HBS buffer. Fractions containing RBD were collected.

The N-terminal peptidase domain of human ACE2 (residues Ser19-Asp615) was expressed and purified by essentially the same protocol used for the SARS-CoV-2 RBD. To purify the SARS-CoV-2 RBD-ACE2 complex, ACE2 was incubated with RBD for 1 h on ice in HBS buffer, and the mixture was then subjected to gel filtration chromatography. Fractions containing the complex were pooled and concentrated to 13 mg/ml.

Crystallization and data collection

Crystals were successfully grown at room temperature in sitting drops, over wells containing 100 mM MES, pH 6.5, 10% PEG5000 mme, 12% 1-propanol. The drops were made by mixing 200 nL SARS-CoV-2 RBD-ACE2 complex in 20 mM Tris pH 7.5, 150 mM NaCl with 200 nL well solution. Crystals were harvested, soaked briefly in 100 mM MES, pH 6.5, 10% PEG5000mme, 12% 1-propanol, 20% glycerol, and flash-frozen in liquid nitrogen. Diffraction data were collected at 100 K and at a wavelength of 1.07180 Å on the BL17U1 beam line of the Shanghai Synchrotron Research Facility (SSRF). Diffraction data were auto-processed with aquarium pipeline and the data processing statistics are listed in the Extended Data Table 1[24].

Structure determination and refinement

The structure was determined by the molecular replacement method with PHASER in CCP4 suite[25]. The search models are ACE2 extracellular domain and SARS-CoV RBD (PDB code 2AJF). Density map improvement by atoms update and refinement was performed with ARP/wARP[26]. Subsequent model building and refinement were performed using COOT and PHENIX, respectively[27,28]. Final Ramachandran statistics: 96.44% favoured, 3.56% allowed and 0.00% outliers for the final structure. The structure refinement statistics are listed in the Extended Data Table 1. All structure figures were generated with PyMol[29].

Surface Plasmon Resonance (SPR) experiments

ACE2 was immobilized to a CM5 sensorchip (GE Healthcare) to a level of ~500 response units (RUs) using a Biacore T200 (GE Healthcare) and a running buffer composed of 10 mM HEPES pH 7.2, 150 mM NaCl and 0.05% Tween 20. Serial dilutions of SARS-CoV-RBD and SARS-CoV-2-RBD were flowed through with a concentration ranging from 62.5 to 1.9 nM. The resulting data were fit to a 1:1 binding model using Biacore Evaluation Software (GE Healthcare).

Reporting summary

Further information on research design is available in the Nature Research Reporting Summary linked to this paper.

Data availability

The coordinates and structure factor files for the SARS-CoV-2 RBD-ACE2 complex were deposited in the Protein Data Bank with accession code 6M0J.

24. Yu, F. et al. Aquarium: an automatic data-processing and experiment information management system for biological macromolecular crystallography beamlines. *J. Appl. Crystallogr.* **52**, 472–477 (2019). https://doi.org/10.1107/s1600576719001183.
25. McCoy, A. J. et al. Phaser crystallographic software. *J. Appl. Crystallogr.* **40**, 658–674 (2007). https://doi.org/10.1107/S0021889807021206.
26. Cohen, S. X. et al. ARP/wARP and molecular replacement: the next generation. *Acta Crystallogr. D Biol. Crystallogr.* **64**, 49–60 (2008). https://doi.org/10.1107/S0907444907047580.
27. Emsley, P. & Cowtan, K. Coot: model-building tools for molecular graphics. *Acta Crystallogr. D Biol. Crystallogr.* **60**, 2126–2132 (2004). https://doi.org/10.1107/S0907444904019158.
28. Adams, P. D. et al. PHENIX: building new software for automated crystallographic structure determination. *Acta Crystallogr. D Biol. Crystallogr.* **58**, 1948–1954 (2002). https://doi.org/10.1107/s0907444902016657.
29. Janson, G., Zhang, C., Prado, M. G. & Paiardini, A. PyMod 2.0: improvements in protein sequence-structure analysis and homology modeling within PyMOL. *Bioinformatics* **33**, 444–446 (2017). https://doi.org/10.1093/bioinformatics/btw638.

Acknowledgements We thank the SSRF BL17U1 beam line for data collection and processing. We thank the X-ray crystallography platform of the Tsinghua University Technology Center for Protein Research for providing the facility support. This work was supported by funds from Beijing Advanced Innovation Center for Structural Biology at Tsinghua University and the National Key Plan for Scientific Research and Development of China (grant number 2016YFD0500307). It is also supported by Tsinghua University Initiative Scientific Research Program (20201080053), National Natural Science Foundation Award (81530065), Beijing Municipal Science and Technology Commission (171100000517-001 and -003), Tencent Foundation, Shuidi Foundation and TH Capital.

Author contributions J.L. and J.G. carried out protein expression, purification, crystallization, diffraction data collection and structure determination with the help of J.Y. and S.S. Q.Z. and X.S. helped in protein expression and purification. S.F., H.Z. and Q.W. helped in crystallization and diffraction data collection. X.W. and L.Z. conceived, designed and directed the study. J.L., J.G., J.Y., S.S., L.Z. and X.W. analyzed the data, made the figures and wrote the manuscript.

Competing interests The authors declare no competing interests.

Additional information

Supplementary information is available for this paper at https://doi.org/10.1038/s41586-020-2180-5.

Correspondence and requests for materials should be addressed to L.Z. or X.W.

Peer review information *Nature* thanks Lijun Rong and the other, anonymous, reviewer(s) for their contribution to the peer review of this work. Peer reviewer reports are available.

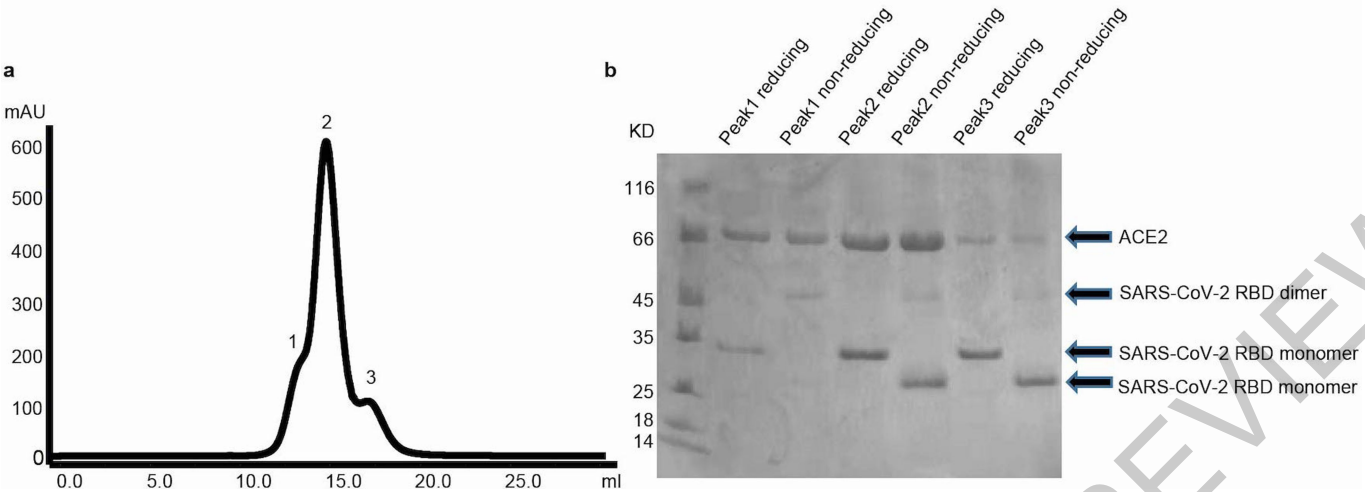

Extended Data Fig. 1 | Purification of SARS-CoV-2 RBD-ACE2 complex. a, Gel filtration chromatography of the complex. **b**, SDS–PAGE gel of the complex.

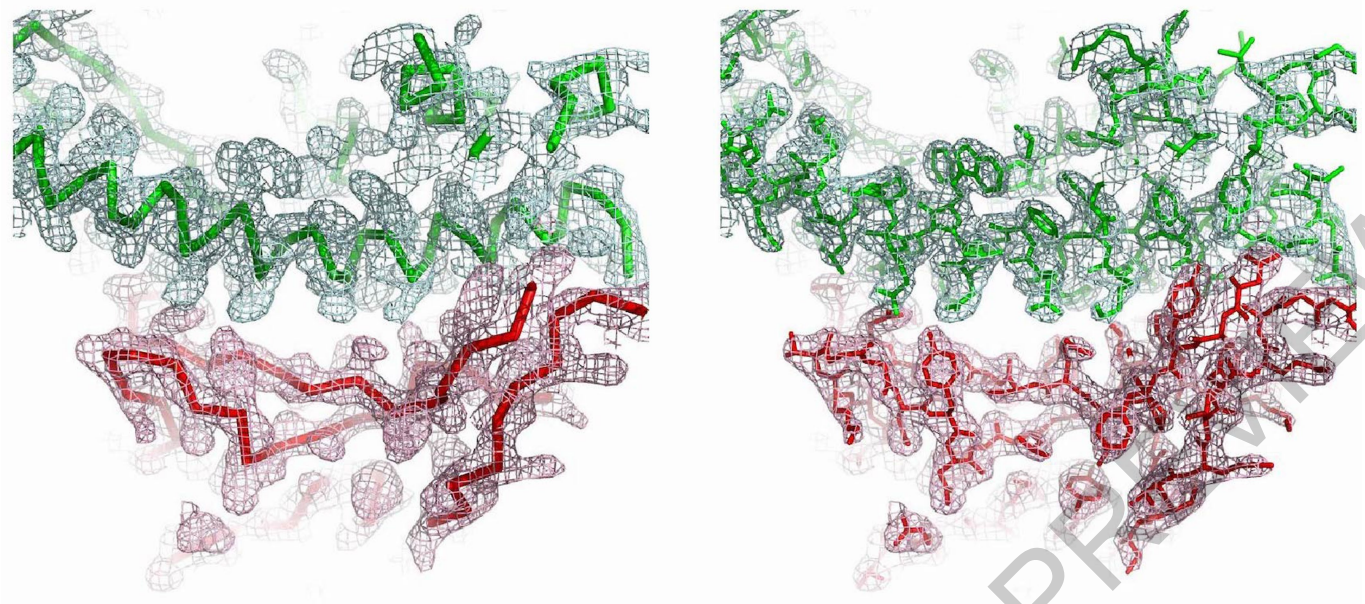

Extended Data Fig. 2 | Electron density map. $2F_O$-F_C electron density map contoured at 1.5σ at the binding interface between SARS-CoV-2 RBD (red) and ACE2 (green).

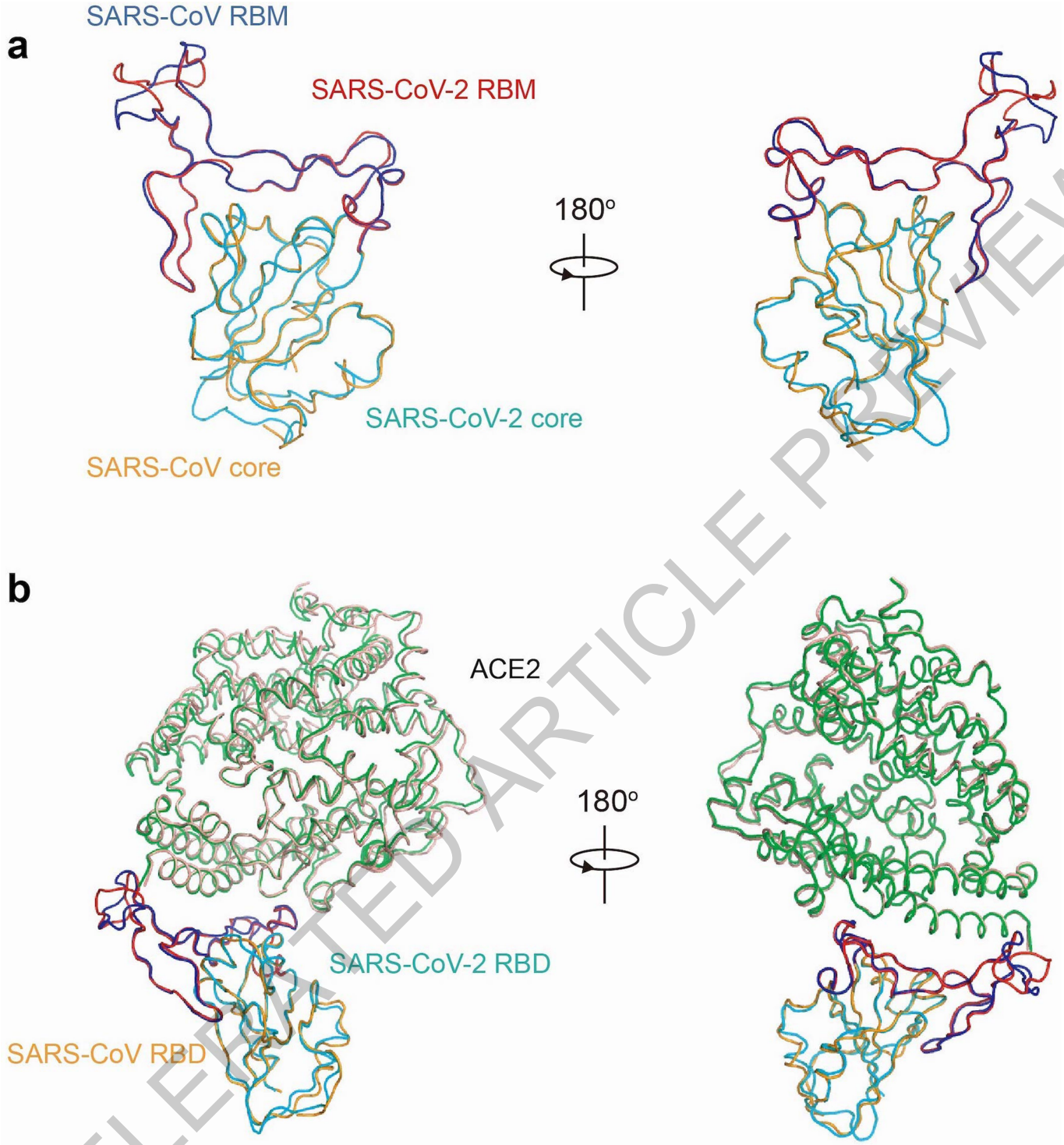

Extended Data Fig. 3 | Structural comparisons of SARS-CoV-2 and SARS-CoV RBDs and their binding modes to ACE2 receptor. a, Alignment of the SARS-CoV-2 RBD (core in cyan and RBM in red) and SARS-CoV RBD (core in orange and RBM in blue) structures. **b**, Structural alignment of SARS-CoV-2 RBD-ACE2 and SARS-CoV RBD-ACE2 complexes. SARS-CoV-2 RBD is colored cyan and red, its interacting ACE2 is colored green. SARS-CoV RBD is colored orange and blue, its interacting ACE2 is colored salmon. The PDB code for SARS-CoV RBD-ACE2 complex: 2AJF.

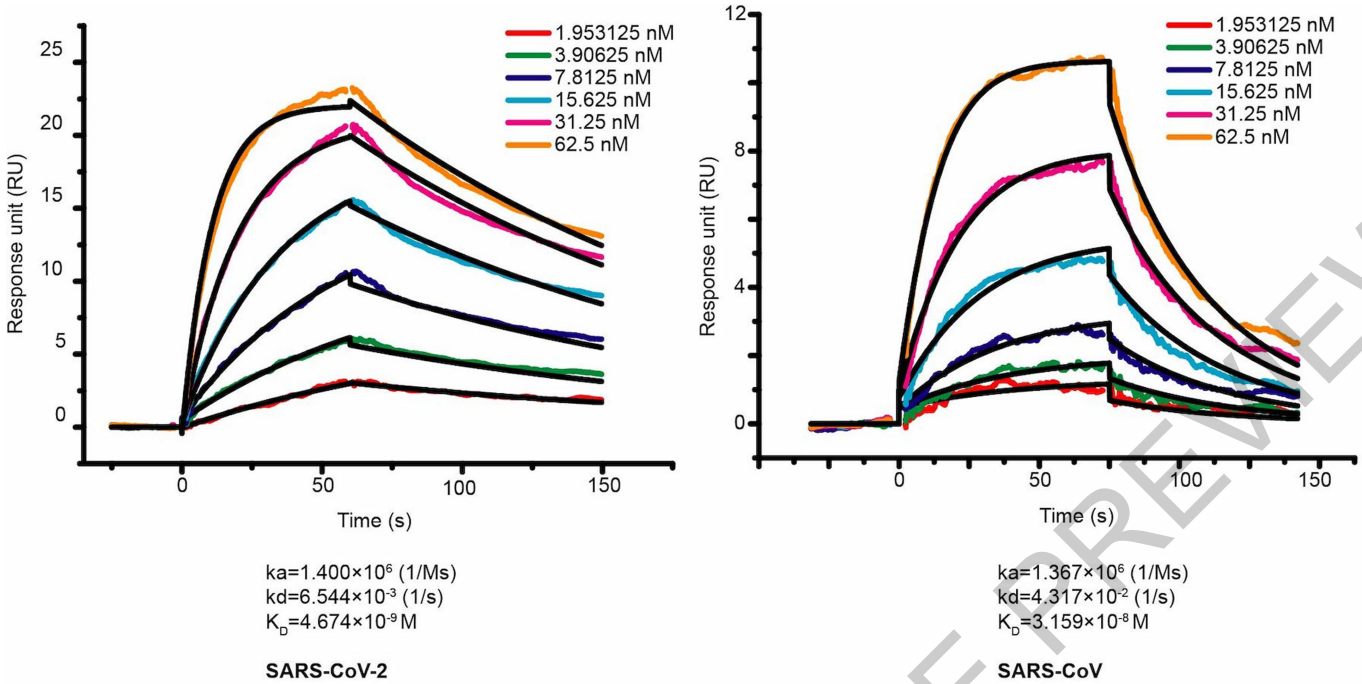

Extended Data Fig. 4 | SPR sensorgrams. Binding curves of immobilized human ACE2 with SARS-CoV-2 RBD (left) and SARS-CoV RBD (right). Data are shown as different colour lines and the best fit of the data to a 1:1 binding model is shown in black.

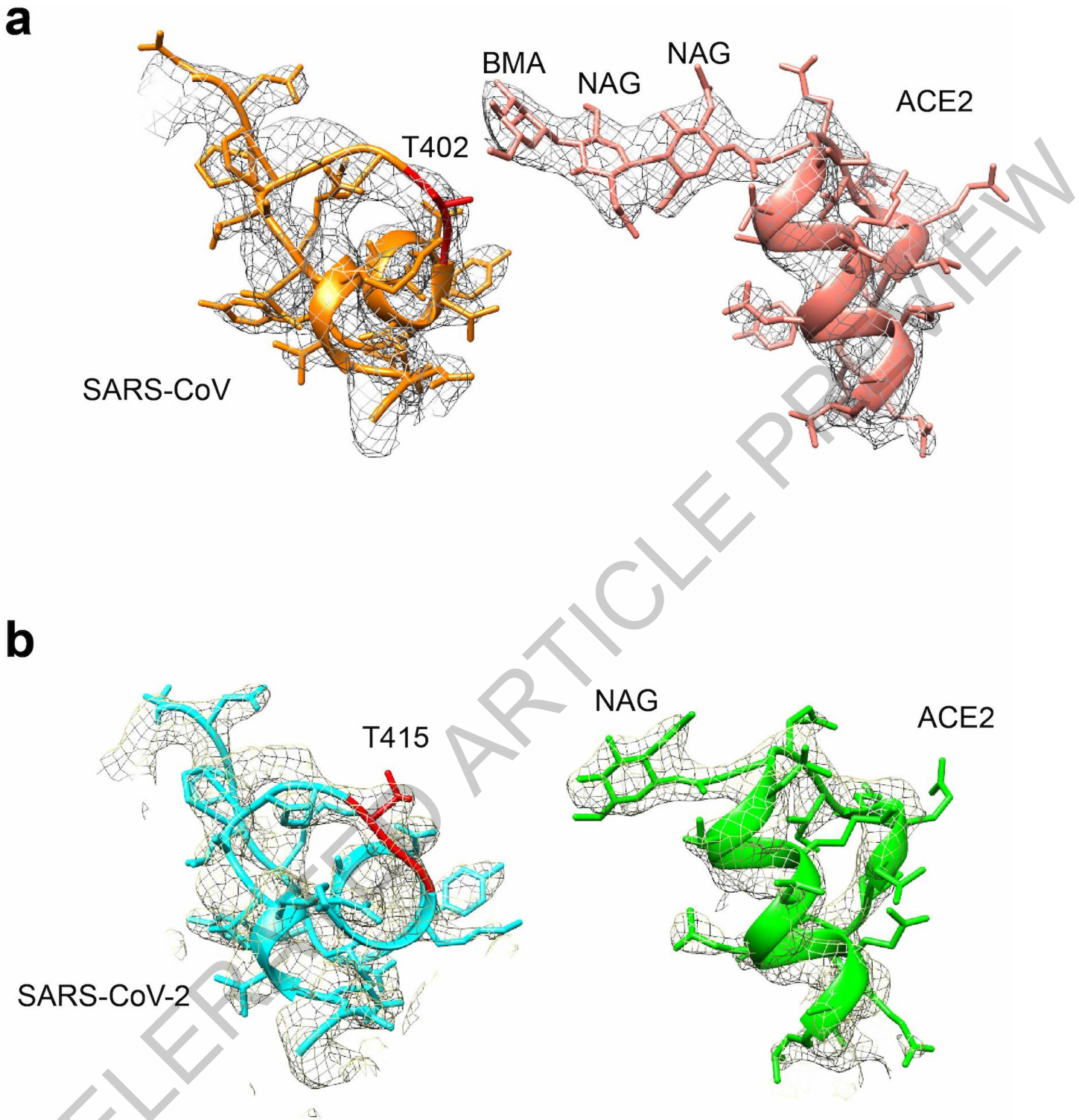

Extended Data Fig. 5 | Asn90-linked glycans of the ACE2. a, The interface between Asn90-linked glycans of the ACE2 (salmon) and SARS-CoV RBD (orange). **b**, The interface between Asn90-linked glycan of the ACE2 (green) and SARS-CoV-2 RBD (cyan). $2F_O$-F_C electron densities contoured at 1.5σ were also shown.

Extended Data Table 1 | Data collection and refinement statistics

	SARS-CoV RBD-ACE2
Data collection	
Space group	$P4_12_12$
Cell dimensions	
a, *b*, *c* (Å)	104.67, 104.67, 228.72
α, β, γ, (°)	90, 90, 90
Resolution (Å)	53.1-2.45(2.54-2.45) *
R_{sym} or R_{merge}	0.118(2.70)
I / sI	24.2(1.7)
Completeness (%)	99.90(99.98)
Redundancy	26.1(27.3)
Refinement	
Resolution (Å)	53.1-2.45
No. reflections	47555
R_{work} / R_{free}	19.6/23.7
No. atoms	
Protein	6419
Ligand/ion	57
Water	80
B-factors	
Protein	64.7
Ligand/ion	91.4
Water	58.1
R.m.s. deviations	
Bond lengths (Å)	0.008
Bond angles (°)	1.21

One crystal was used.
*Values in parentheses are for highest-resolution shell.

Extended Data Table 2 | Contacting residues (a distance cutoff 4 Å) at the SARS-CoV-2 RBD/ACE2 and SARS-CoV RBD/ACE2 interfaces

SARS-CoV-2 RBD	ACE2	SARS-CoV RBD	ACE2
K417	Q24	R426	Q24
G446	T27	Y436	T27
Y449	F28	Y440	F28
Y453	D30	Y442	K31
L455	K31	L443	H34
F456	H34	L472	E37
A475	E35	N473	D38
F486	E37	Y475	Y41
N487	D38	N479	Q42
Y489	Y41	G482	L45
Q493	Q42	Y484	L79
G496	L79	T486	M82
Q498	M82	T487	Y83
T500	Y83	G488	Q325
N501	N330	I489	E329
G502	K353	Y491	N330
Y505	G354		K353
	D355		G354
	R357		D355
	R393		R357

nature research

Corresponding author(s): *Double-blind peer review submissions: write DBPR and your manuscript number here instead of author names.*

Last updated by author(s): *YYYY-MM-DD*

Reporting Summary

Nature Research wishes to improve the reproducibility of the work that we publish. This form provides structure for consistency and transparency in reporting. For further information on Nature Research policies, see Authors & Referees and the Editorial Policy Checklist.

Statistics

For all statistical analyses, confirm that the following items are present in the figure legend, table legend, main text, or Methods section.

n/a	Confirmed
☒	☐ The exact sample size (*n*) for each experimental group/condition, given as a discrete number and unit of measurement
☒	☐ A statement on whether measurements were taken from distinct samples or whether the same sample was measured repeatedly
☒	☐ The statistical test(s) used AND whether they are one- or two-sided *Only common tests should be described solely by name; describe more complex techniques in the Methods section.*
☒	☐ A description of all covariates tested
☒	☐ A description of any assumptions or corrections, such as tests of normality and adjustment for multiple comparisons
☒	☐ A full description of the statistical parameters including central tendency (e.g. means) or other basic estimates (e.g. regression coefficient) AND variation (e.g. standard deviation) or associated estimates of uncertainty (e.g. confidence intervals)
☒	☐ For null hypothesis testing, the test statistic (e.g. *F*, *t*, *r*) with confidence intervals, effect sizes, degrees of freedom and *P* value noted *Give P values as exact values whenever suitable.*
☒	☐ For Bayesian analysis, information on the choice of priors and Markov chain Monte Carlo settings
☒	☐ For hierarchical and complex designs, identification of the appropriate level for tests and full reporting of outcomes
☒	☐ Estimates of effect sizes (e.g. Cohen's *d*, Pearson's *r*), indicating how they were calculated

Our web collection on statistics for biologists contains articles on many of the points above.

Software and code

Policy information about availability of computer code

Data collection	NCBI was used for downloading the published SARS-CoV-2 sequences to do the research
Data analysis	Aquarium pipeline, CCP4 v7.0, COOT 0.8.6 and PHENIX 1.15.2-3472 were used at the determination of complex structure for data processing , model building and refinement. PyMOL 1.8.x was used to generate the structural figures.

For manuscripts utilizing custom algorithms or software that are central to the research but not yet described in published literature, software must be made available to editors/reviewers. We strongly encourage code deposition in a community repository (e.g. GitHub). See the Nature Research guidelines for submitting code & software for further information.

Data

Policy information about availability of data

All manuscripts must include a data availability statement. This statement should provide the following information, where applicable:

- Accession codes, unique identifiers, or web links for publicly available datasets
- A list of figures that have associated raw data
- A description of any restrictions on data availability

Crystal structure presented in this work has been deposited in the Protein Data Bank (PDB) and are available with accession codes 6M0J.

Field-specific reporting

Please select the one below that is the best fit for your research. If you are not sure, read the appropriate sections before making your selection.

☒ Life sciences ☐ Behavioural & social sciences ☐ Ecological, evolutionary & environmental sciences

Life sciences study design

All studies must disclose on these points even when the disclosure is negative.

Sample size	Two separate proteins were purified and formed a complex.
Data exclusions	No data excluded.
Replication	The crystal of the complex were obtained in duplicate. All attempts at replication were successful.
Randomization	N/A
Blinding	N/A

Reporting for specific materials, systems and methods

We require information from authors about some types of materials, experimental systems and methods used in many studies. Here, indicate whether each material, system or method listed is relevant to your study. If you are not sure if a list item applies to your research, read the appropriate section before selecting a response.

Materials & experimental systems

n/a	Involved in the study
☒	☐ Antibodies
☐	☒ Eukaryotic cell lines
☒	☐ Palaeontology
☒	☐ Animals and other organisms
☒	☐ Human research participants
☒	☐ Clinical data

Methods

n/a	Involved in the study
☒	☐ ChIP-seq
☒	☐ Flow cytometry
☒	☐ MRI-based neuroimaging

Eukaryotic cell lines

Policy information about cell lines

Cell line source(s)	SF9 and Hi5 cells were bought from ATCC
Authentication	SF9：refered to website: https://www.atcc.org/products/all/CRL-1711.aspx Hi5：refered to website These two cell lines are all available in commercial company.
Mycoplasma contamination	We confirm that all cell lines were negative for mycoplasma contamination
Commonly misidentified lines (See ICLAC register)	No commonly misidentified cell lines were used